ACS APPLIED MATERIALS & INTERFACES

Research Article

www.acsami.org

Modulating Contact Angle Hysteresis To Direct Fluid Droplets along a Homogenous Surface

Mingxiang Luo, Rohini Gupta, and Joelle Frechette*

Chemical and Biomolecular Engineering Department, Johns Hopkins University, 3400 North Charles Street, Baltimore, Maryland 21218, United States

Supporting Information

ABSTRACT: The shape and motion of drops on surfaces is governed by the balance between the driving and the pinning forces. Here we demonstrate control over the motion of droplets on an inclined surface by exerting control over the contact angle hysteresis. The external modulation of contact angle hysteresis is achieved through a voltage-induced local molecular reorganization within the surface film at the solid–liquid interface. We show that tuning contact angle hysteresis alone is sufficient to direct and deform drops when subjected to a constant external driving force, here gravity, in the absence of a pre-defined surface energy gradient or pattern. We also show that the observed stretching and contraction of the drops mimic the motion of an inchworm. Such reversible manipulation of the pinning forces could be an attractive means to direct drops, especially with the dominance of surface forces at micro-/nanoscale.

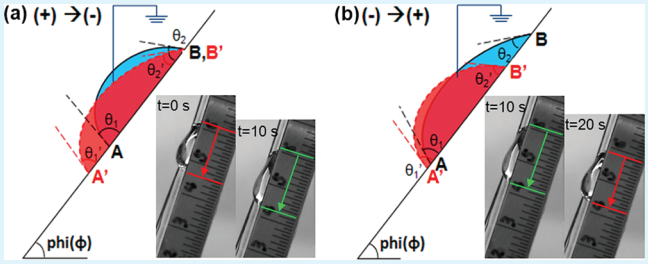

KEYWORDS: *responsive surfaces, contact angle hysteresis, drop motion, wetting*

INTRODUCTION

The dominance of surface properties at the micro-/nanoscale has opened the door for the use of surface energy as a means to manipulate fluid droplets.[1−3] To manipulate droplets, the fluid–surface interactions need to respond in real time to an external stimulus[4−9] and to experience a surface energy gradient[10−13] in the direction of motion. Hard-coded surface energy gradients for drop motion can be designed via local variations in chemistry,[9,10,14] topography,[15−17] electric field,[4,5] or temperature,[18,19] but motion is often hindered by contact angle hysteresis. Limitations due to contact angle hysteresis can be addressed by using small perturbations[11,13,16,20−24] to provide sufficient energy to overcome contact angle hysteresis and, as a consequence, facilitate the manipulation of droplets on a pre-existing surface gradient. Unlike pre-defined hard-coded surface energy gradients, surfaces with tunable contact angle hysteresis could display enhanced versatility, as they would not require a separate design of the surface energy gradient for different devices. In addition, modulating contact angle hysteresis on demand could lead to the study of ongoing issues in interfacial science, such as drop motion on heterogeneous surfaces, the pinning of drops on surfaces, and the origin of contact angle hysteresis.

Contact angle hysteresis is a manifestation of the pinning of the triple contact line of drops on surfaces and leads to a threshold force that must be overcome for the initiation of drop motion.[25,26] For instance, the presence of contact angle hysteresis leads to the appearance of a non-zero critical tilt angle (ϕ_c) for a drop to slide down an inclined plane due to gravity (Figure 1a). At this critical tilt angle, the component of the gravitational force along the incline ($F_g = mg \sin \phi_c$) balances the pinning force ($F_p = \gamma_{LV} w[\cos \theta_{rec} - \cos \theta_{adv}]$), where mg is the gravitational force, γ_{LV} is the liquid–vapor surface tension, w is the width of the drop perpendicular to motion , and θ_{adv} and θ_{rec} are the advancing and receding contact angles, respectively.[27,28] Consider a drop with Bo = gravity/surface tension = $(\rho g l_c^2 \sin \phi)/\gamma_{LV} > 1$ placed on an inclined surface with arbitrary contact angle hysteresis, where ρ is the density of the liquid, l_c is the characteristic length of the droplet, and ϕ is the tilt angle.[29] The gravitational force will deform the drop such that it acquires a larger contact angle at the front end (θ_1) than at the rear end (θ_2). As long as $\theta_1 < \theta_{adv}$ and $\theta_2 > \theta_{rec}$, the drop remains stationary as gravity is not sufficient to overcome the pinning force. At the critical tilt angle for incipient drop motion the values of the contact angles correspond to the advancing angle at the front end and the receding angle at the rear end, and the whole drop accelerates as it slides down the incline. Therefore, balance of the pinning and gravitational force dictates the critical tilt angle required to initiate the motion of droplets.

Here we demonstrate a different mechanism whereby the motion of droplets on an inclined surface, when subjected to a uniform force field (here gravity at a fixed tilt angle), is controlled by tuning the contact angle hysteresis. The modulation of contact angle hysteresis is achieved by a local molecular reorganization at the solid–liquid interface in

Received: November 8, 2011
Accepted: January 5, 2012
Published: January 5, 2012

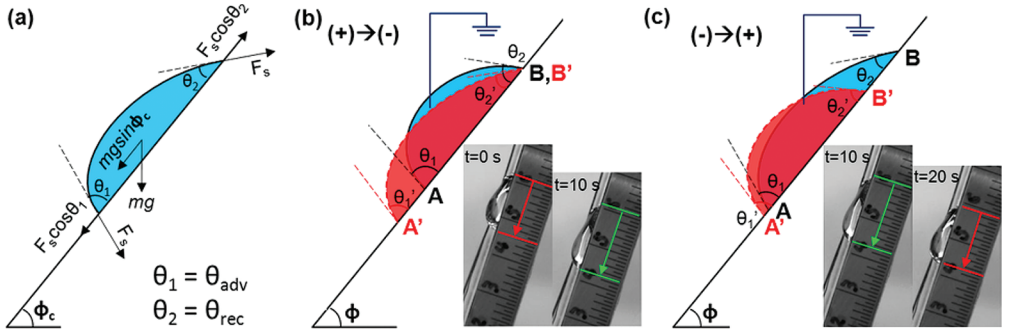

Figure 1. (a) Drop on inclined plane at incipient motion. (b, c) Illustration of the change in drop shape due to potential-induced change in contact angle hysteresis. Schematic illustration and picture of (b) the stretching of the drop due to the pinning of the rear end caused by an increase in CAH when the potential is switched from positive to negative and (c) the contraction of a liquid drop due to a decrease in CAH when the potential goes from negative to positive. Cycles of (b) and (c) lead to the drop "inchworm" crawling motion.

response to an electric potential without any pre-defined patterned electrodes. We also demonstrate that modulation of contact angle hysteresis can be employed to stretch and contract a droplet such that its motion mimics the locomotion of an inchworm and that the observed inchworm motion can be understood in terms of pinning of the front or rear end of the drops as they slide down the incline. By demonstrating how external modulation of contact angle hysteresis influences drop motion, we present an alternative and fundamentally different strategy to move drops on surfaces that requires no hard-coded patterns or pre-defined surface energy gradients.

EXPERIMENTAL METHODS

Materials. 16-Mercaptohexadecanoic acid (MHA, 99.8%), carbon tetrachloride (99.99%), potassium chloride (99.0%), potassium perchlorate (99%), acetonitrile (99%), and tetrapentylammonium hydroxide ($[CH_3(CH_2)_4]_4N^+OH^-$, TPeAOH), received as 1 M aqueous solution, were used as received from Sigma-Aldrich. Dimethyl sulfoxide, KOH pellets, HCl, H_2SO_4, and H_2O_2 were purchased from Fisher Scientific. Mica sheets were obtained from S&J Trading. Gold wire (99.99%) was purchased from Kurt J. Lesker. Chromium (99.99%) was purchased from Alfa Aesar. Ethanol (200 Proof) was used as received from Warner-Graham Co. Purified water (18.3 MΩ·cm) was obtained from a Milli-Q Gradient system.

Synthesis of Responsive Monolayers. The responsive monolayer consists of low-density mercaptohexadecanoic acid (LD-MHA). The films were obtained by performing ion-exchange of monolayers made from ion pairs of tetrapentylammonium and mercaptohexadecanoic acid. The solution condition followed for the formation of the ion-pair monolayers is described in our previous work[30−32] with the only difference being the use of a higher ratio of TPeAOH/MHA (6:1 vs. 4:1) to facilitate ion-pair formation. The LD-MHA monolayers obtained were characterized via IR spectroscopy and contact angle measurements.

Control of Applied Potential. A standard three electrode arrangement was used to set the applied potential on the LD-MHA covered surface. In this arrangement, the LD-MHA/gold substrate acted as the working electrode, a Ag/AgCl wire was used as a reference electrode, and a platinum wire was used as the counter electrode. The potential of the gold substrate, relative to the Ag/AgCl wire, was controlled using a CHI 650B electrochemical workstation (CH Instruments). The potential was switched either between −0.30 V (reported as negative potential in the text) and 0.20 V (reported as positive potential in the text) or between −0.34 V and 0.26 V with respect to the pseudo Ag/AgCl reference electrode. The potential of the pseudo reference electrode was measured to be 0.20 ± 0.02 V with respect to a standard Ag/AgCl(3M) reference electrode.

Dynamic Contact Angle Measurements. Advancing and receding contact angle measurements at different applied potentials were performed at room temperature with a liquid drop of 1 mM KCl with 25% acetonitrile (v/v) at pH 11 (pH was adjusted with KOH) by the captive drop technique.[33] Expansion and contraction of the droplet at a rate of 6 μL/min was achieved using a syringe pump (World Precision Instruments) via a glass capillary inserted in the drop (the working and counter electrodes were inserted in the glass capillary). Receding and advancing contact angles were denoted as the angles right before the three-phase contact line receded or advanced over the surface, respectively (see Figure 2a). Prior to measurements, samples were rinsed with ethanol, followed by a brief rinse with Milli-Q water, and dried with a stream of nitrogen gas prior to measurement. Values for the advancing and receding angles given are averaged from at least nine locations on three samples; at least three measurements were made on each location. All the values are reported as average ± standard deviations.

Experimental Setup for Drop Motion Experiments. The LD-MHA covered gold substrate was mounted on a homemade plate with two parallel wires above the gold surface: the Ag/AgCl reference and the Pt counter electrode (see Supporting Information, Figure S1). The plate was placed on a homemade device with a microcontroller to adjust tilt angles. Before and between experiments, the surfaces were cleaned with ethanol, followed by a brief rinse with Milli-Q water, and dried with a stream of nitrogen gas. Images of the droplet were taken using a digital camera (Navitar 7000, Nikon) at a frame rate of 30 fps and analyzed using ImageJ software.

Current Decay Measurements. Potential step measurements were performed in 1 mM KCl with 25% acetonitrile (v/v, pH 11) electrolyte solutions at room temperature after de-aerating the electrolyte with water-saturated ultrapure nitrogen gas for 45 min. The test samples were mounted to a flat-cell (Princeton Applied Research), with a fixed working electrode area of 1 cm^2, Ag/AgCl/3 M KCl (aq) reference electrode (CH Instruments) and platinum mesh counter electrode. Evolution of current through the film was measured at DC bias potentials +0.4 and −0.1 V with respect to the standard calomel electrode (SCE), using a CHI 650B electrochemical workstation (CH Instruments). After measurement, the time constant was derived from exponential fits of the current−time decay. Reported values represent the mean of measurements in five cycles.

RESULTS AND DISCUSSION

Measurements of Contact Angle Hysteresis. We employ thin films that display large change in contact angle hysteresis with applied potential. The surface chemistry consists of a low-density self-assembled monolayer of mercaptohexadecanoic acid (LD-MHA) deposited on a smooth gold surface. The surface coverage (i.e., the molecular footprint of an individual MHA chain) estimated from desorption experiments was found to be 0.57 ± 0.10 nm^2/molecule.[32] The submonolayer surface coverage is obtained by sterically hindering the packing of the MHA on the surface via ion-pair formation in solution[30] and results in enhanced conformational

dx.doi.org/10.1021/am201557k | ACS Appl. Mater. Interfaces 2012, 4, 890−896

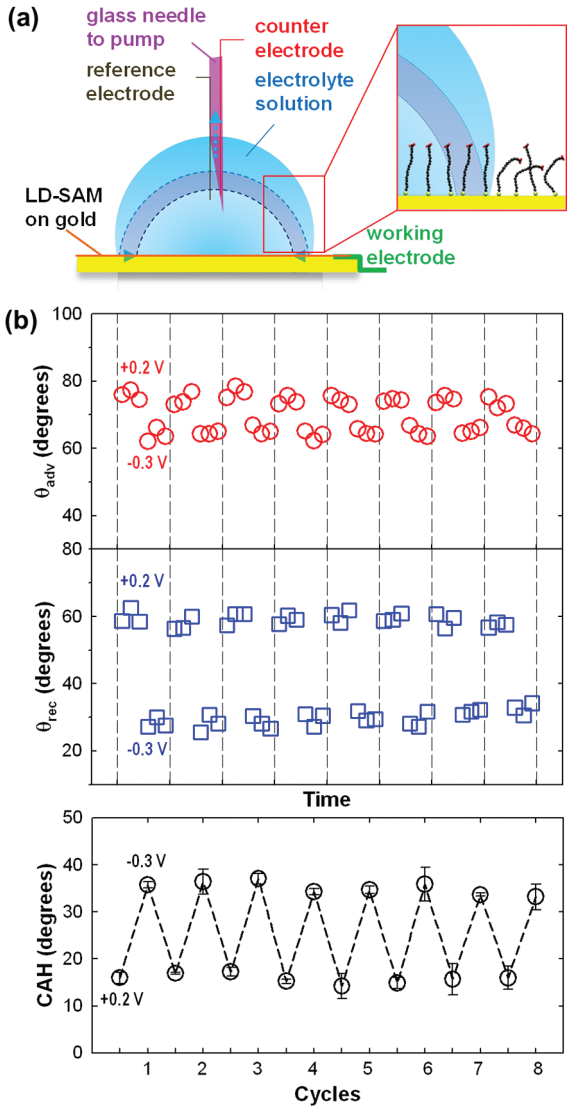

Figure 2. Measurement of advancing and receding contact angles and contact angle hysteresis (CAH) on LD-SAMs using 1 mM KCl electrolyte solution with acetonitrile (75:25 v/v at pH 11). (a) Schematic illustration of advancing and receding contact angle measurement setup. Inset shows how the LD-SAMs exposed within the drop are more sensitive to external stimulus. (b) Reproducible measurements of advancing contact angle, receding contact angle, and CAH. Eight switching cycles between +0.20 V and −0.30 V are shown. The drawn lines are to guide the eye.

freedom of the chains (see Figure 2a illustrating two different conformations at two locations). This conformational freedom allows the chains to rearrange with an applied potential and leads to significant changes in the wettability of the monolayers.[30,31,34] Dynamic contact angle measurements show that for the films employed here the contact angle hysteresis reproducibly changes by 20 ± 1° upon a difference of 0.5 V in applied potential. In average the contact angle hysteresis switches between 16 ± 1° at positive potential and 36 ± 3° at negative potential. Our measurements also show that the observed change in contact angle hysteresis is reproducible for at least eight cycles (Figure 2b). For the two sets of potential steps investigated here the change in contact angle hysteresis was consistently at 20° (Table 1).

Table 1. Measurement of Dynamic Contact Angle at Two Similar Sets of Potentials[a]

	set 1		set 2	
angles (deg)	+0.26 V	−0.34 V	+0.2 V	−0.3 V
θ_{adv}	80 ± 3	73 ± 2	75 ± 1	65 ± 2
θ_{rec}	62 ± 1	31 ± 2	59 ± 1	29 ± 2
CAH	19 ± 2	41 ± 3	16 ± 1	36 ± 3
ΔCAH	22 ± 3		20 ± 3	

[a]The result shown in Set 1 is the average from 42 advancing or receding measurements on three samples, and the result in Set 2 is the average from 36 measurements on five samples. At least three potential switching cycles were performed on each sample, and three advancing and receding angles were measured at each potential. The reported CAH is the average of difference between advancing and receding angles obtained from multiple measurements and samples. The reported ΔCAH is the average of difference in CAH at two different potentials obtained from multiple measurements and samples.

Most of the change in contact angle hysteresis comes from changes in the receding angle ($\Delta\theta_{rec}$ = 31 ± 2° vs $\Delta\theta_{adv}$ = 9 ± 2°, see Table 1), which is consistent with contact line motion on a smooth but chemically heterogeneous surface.[34−36] While we do not have pre-defined chemical heterogeneities on the surface (or sudden change in surface roughness), we suspect that the conformational freedom within the monolayer allows the chains to adopt a different configuration at the solid−liquid interface (higher energy) than at the solid-vapor interface (lower energy) (see Figure 2a). In other terms, the surface effectively becomes chemically heterogeneous when it is in contact with a fluid, and the scale of this heterogeneity is the size of the drop. Moreover, the conformational change at the solid−liquid interface is modulated by the potential (while the potential outside the drop is, to a large extent, unaffected by the applied potential), and thus this modulation leads to a large change in receding angle. It is interesting to note that we do also observe a small but significant change in advancing angle with applied potential, which has not been observed previously.[34] A better understanding of the dynamic of the molecular reorganization with applied potential and how it relates to the motion of the triple contact line is necessary to explain this change.

The voltage-induced change in contact angle hysteresis is quite different from the absence of change in contact angle hysteresis observed in electrowetting (or electrowetting on dielectric, EWOD).[37] In EWOD it has been established that the spreading of a drop with applied potential is observed (change in the static contact angle) while the magnitude of the contact angle hysteresis remains unaffected by the potential.[38−40] This is due to the fact that in EWOD the spreading of a drop on the dielectric in response to the applied field is due to fringe fields near the triple contact line, which results from the non-uniform charge distribution and associated Maxwell stress. Furthermore, in electrowetting the microscopic contact angle remains constant and equal to the values bound by the contact angle hysteresis under no applied potential, and it is only far from the solid−liquid interface that the drop remains a spherical cap whose apparent contact angle is described by the electrowetting equation. Near the triple contact line the curvature diverges and the microscopic contact angle remains between the advancing and the receding angles as the applied potential changes.[37,41−43] In constrast, the mechanism at play for the change in wetting properties with applied potential in this work is a molecular

rearrangement of the chains and not an electromechanical stress forcing the drop to spread.[31,34] As a consequence, for the films employed here we observe no significant change in the static contact angle and a significant change in contact angle hysteresis as the potential is changed. Finally the mechanism for contact angle change observed here is also fundamentally different from other mechanisms aimed at overcoming hysteresis using vibrations,[11,13] electrical pulses,[21] or high AC frequency in electrowetting.[22]

Modulation of Contact Angle Hysteresis To Control Drop Motion. We consider the scenario where the control of contact angle hysteresis can be employed to direct drop motion. Consider the case of the drop on an inclined plane discussed in the Introduction. Instead of changing the tilt angle here we control the pinning force instantaneously due to an external trigger (here an applied potential) while the tilt angle is fixed (constant driving force). A stimuli-dependent change in the pinning force would effectively modify the critical tilt angle for incipient drop motion, which in turn could alter drop motion and cause drop deformation. While in many cases the trigger would lead to no change in the drop's state of motion, more interestingly the stimulus can sometimes pin or free the triple contact line at one or both ends of the drop (see Figure 1b,c). These changes can lead to four distinct macroscopic outcomes for the drop caused by the change in contact angle hysteresis. First, a near instantaneous arrest of a moving drop will be observed if the front and rear end suddenly become pinned. Second, an onset of drop sliding will be observed if a stimulus frees both the front and the rear end of a stationary drop. Third, stretching prior to drop arrest will occur if the rear end of a drop becomes pinned while the front end is free. Such behavior would be seen, for example, with a decrease in the receding angle (Figure 1b). In that case the stretching would lead to drop arrest as the contact angle at the front end will ultimately decrease below the advancing angle. Finally, contraction prior to motion will be observed if the rear end is freed while the front end remains pinned (for example, when the receding angle is increased, see Figure 1c). In this case the contraction of the drop would lead to an increase in the contact angle at the front end and ultimately lead to drop sliding when the contact angle at the front end reaches the advancing angle. Therefore, it is expected that tuning contact angle hysteresis can lead to deformation (stretching or contraction) of a drop which could trigger the onset of motion or arrest of a sliding drop.

Our experiments with drops of $Bo \sim 3$ confirm that external control over the pinning force can indeed be employed to initiate and impede drop motion on a homogeneous surface. A drop of 30 μL placed on a plane tilted at 85° stays at rest at a negative potential (Figure 3a) but slides down when the polarity of the applied potential is switched to positive (Figure 3b). This observation demonstrates that contact angle hysteresis can function as an "on-off" switch to control the drop motion and is consistent with the measured reduction in contact angle hysteresis when the applied potential is changed from negative to positive values. Similarly, the modulation of the pinning force can also impede the motion of a sliding drop upon switching the potential from positive to negative values. Unfortunately, the capillary force caused by the electrical wires on top of the drop prevents a quantitative comparison with the predicted change in critical tilt angle associated with the independently measured change in pinning force. The first two scenarios discussed earlier (instantaneous arrest or sliding of the drop) cannot be observed with our surfaces as they require the values of the advancing and receding angles to change in opposite directions in response to the external stimulus (which we do not observe). The predicted drop deformation (the third and fourth scenario of drop response) caused by changing the pinning force can be clearly observed in our experiments. Figure 4 shows that by alternating the pinning force back and forth between the two states the drop experiences significant stretching and contraction as it responds to the switching potential and slides down the inclined plane. Repeated stretching and contraction of the drop as the potential is reversibly switched makes the motion of the drop mimic the crawling of an inchworm (see Figure 4a and Movie S1 in Supporting Information).

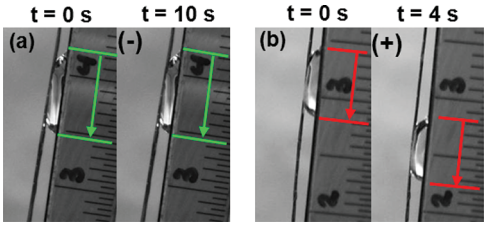

Figure 3. Contact angle hysteresis as an "on-off" switch to initiate drop motion. Pictures show (a) a drop (~30 μL) that stays at rest on an 85° incline when a negative potential is applied and (b) a drop of the same volume slides when the potential is positive.

The stretching, contraction, and overall motion of the drops were characterized by monitoring the changes in their base length and absolute positions at the front and rear ends (Figure 4b–d). At negative potentials the increase in the pinning forces causes the drop to stretch and ultimately come to rest: the front end advances, the rear end stays pinned, and the base length increases (Figure 4b–d). At positive potentials we observe the predicted contraction associated with a decrease in the pinning force: there is motion of the rear end of the drop while the front end is still pinned along with an overall decrease in base length. An overall drop motion that would be associated with a drop contraction is not observed for the case shown in Figure 4, as the tilt angle and volume of the drop were selected to satisfy the condition of incipient motion of the drop (zero velocity).[44,45] For larger drop volume or tilt angle the gravitational force exceeds the pinning force, which leads to net drop motion in the direction of driving force. In these cases we observe sliding of the drop following (or during) the contraction at positive potentials (see Movie S2 in Supporting Information).

The drop experiences significant stretching and contraction as it responds to the switching potential and slides down the inclined plane (Figure 4a). The drop motion when changing the applied potential resembles the crawling of an inchworm (see Movie S1 in Supporting Information). Changes in the base length and absolute positions of the front and rear end of the drop have been used to characterize the drop stretching, contraction, and overall motion (Figure 4b,d). The images indicate that at positive potential the rear end of the drop initially recedes towards the center of the drop (contraction) and then stops moving. At negative potential, the front end of the drop advances while the rear end stays pinned (stretching), and eventually the drop stops moving (Figure 4b,d). The stretching and contraction cycles can be repeated multiple times, making the drop stop and go on demand on the surface. Analysis of the drop base length indicates that the drop

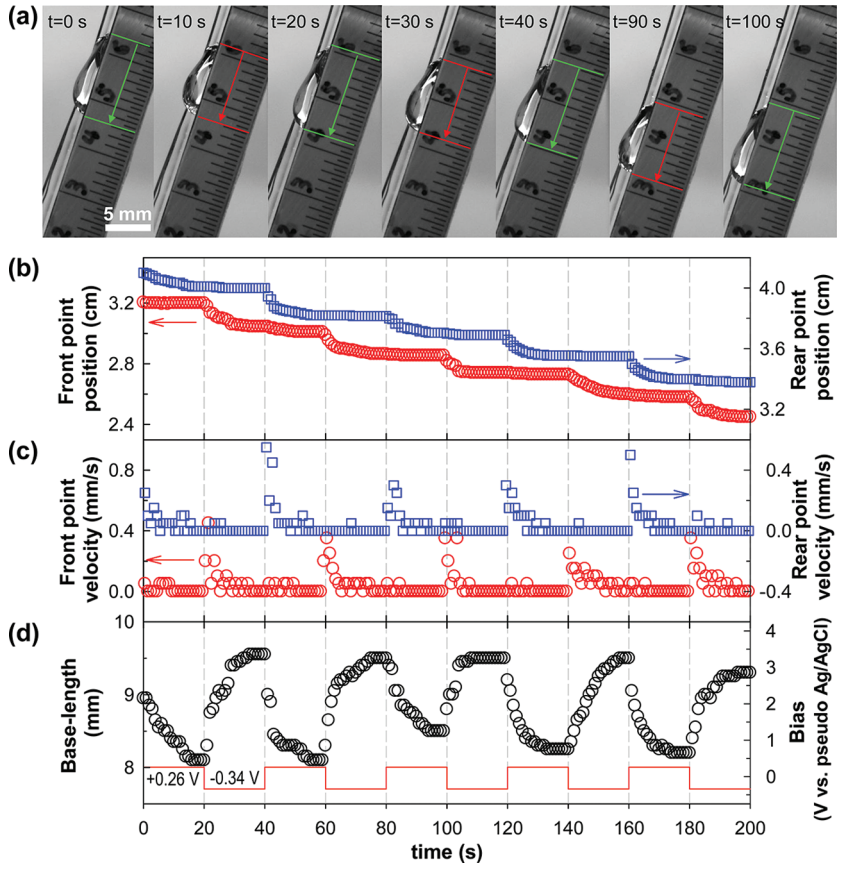

Figure 4. In situ observation of a liquid drop continuous "inchworm" motion down an incline directed by changes in CAH. (a) Extracted frames at 10 s intervals show the stretching and contraction of the liquid drop. The liquid drop stays at rest at negative potential prior to switching to positive potential at t = 0 s. The potential is switched alternatively between positive and negative at 10 s intervals; analysis of (b) front (red circles) and rear (blue squares) end position, (c) velocity, and (d) base length (black circles in lower panel) at different times with 20 s switching intervals. The red solid line represents the applied DC. The plateau indicates when the stretching and contraction are completed, and the shape of the drop reaches steady-state (static or sliding). Here, pinning at either the front or rear end is defined as a zero velocity (Figure 4c).

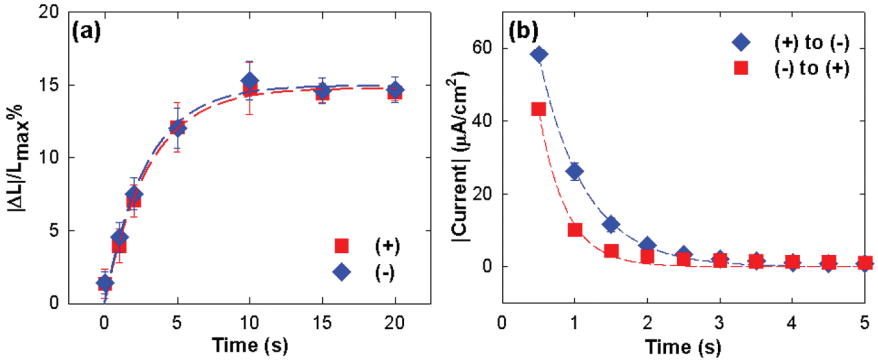

Figure 5. (a) Time dependence of the relative change in base length at positive and negative potentials. Dashed lines are exponential fits to the data with time constants of τ = 3.01 ± 0.32 s, R^2 = 0.99 (positive applied potential), and of τ = 2.85 ± 0.34 s, R^2 = 0.98 (negative applied potential). (b)Time dependence of decay in charging current for an LD-MHA film upon switching between positive and negative potentials. Dashed lines are exponential fits to the data with time constants of τ = 1.68 ± 0.03 s, R^2 = 0.99 (switching from positive to negative applied potentials), and τ = 0.77 ± 0.02 s, R^2 = 0.99 (switching from negative to positive applied potentials).

stretching at negative potential causes it to decelerate and stop unless the potential is switched back to a positive value (Figure 4c). In addition to controlling the drop motion on an inclined surface, we have also shown that by changing CAH we can control the drop motion in a closed channel device (Figure S2 in Supporting Information).

The entire motion of the drop occurs on a homogeneous inclined surface without any hard-coded surface energy gradient, patterned electrodes, or change in tilt angle when subjected to a constant external driving force and is solely driven by potential-induced changes in the contact angle hysteresis caused by a molecular reorganization. The observed features of Figure 4 can be attributed to the transition of the droplet as it adapts to the change in contact angle hysteresis. For $\theta_1 < \theta_{adv}$ and $\theta_2 > \theta_{rec}$, the drop is stationary as gravity is not sufficient to overcome the pinning force. At the critical tilt

dx.doi.org/10.1021/am201557k | ACS Appl. Mater. Interfaces 2012, 4, 890–896

angle for motion, the equilibrium values of the contact angles correspond to the advancing angle at the front end and the receding angle at the rear end. Prior to steady state, however, other configurations are accessible and have been observed in our experiments. For $\theta_1 < \theta_{adv}$ and $\theta_2 \leq \theta_{rec}$, the rear end retracts while the front end stays pinned, leading to drop contraction at positive potential, while θ_1 increases to θ_{adv}, at which point the drop slides down the incline. Alternatively for $\theta_1 \geq \theta_{adv}$ and $\theta_2 > \theta_{rec}$, the rear end stays pinned while the front end of the drop advances, leading to drop stretching at negative potential, and stretching stops when $\theta_1 < \theta_{adv}$. In our experiments, we reversibly switch between these two states by altering the polarity of the applied potential, which means that at one potential the drop slides and at another it stops while the stretching and contraction are manifestations of the transition between these two states.

The time scale associated with stretching or contraction in response to the applied potential and switch time interval can be interpreted in terms of interplay of surface forces and inertia. For simplicity, we consider the case shown in Figure 4 where the drop stops after both the stretching and the contraction steps (i.e., incipient motion or zero velocity at positive potential). For switching intervals greater than 10 s, the base length changes by an average of 15 ± 3% for both stretching and contraction, with an abrupt change of 3% within the first second (Figure 5a). A small decrease in base length for the 20 s switching interval is likely due to the evaporation of exposed electrolyte solution drop during the measurement time involved. The change in base length, ΔL, exhibits exponential time dependence $\Delta L(t) = \Delta L_{max}(1 - e^{-t/\tau})$ with a time constant $\tau = 3.0 \pm 0.3$ s. Interestingly, the characteristic time scale for the change in base length is the same for both drop stretching and contraction. The Weber number associated with drop stretching or contraction is significantly less than unity ($We = \rho v^2 l/\gamma$ = inertia/surface tension, $We \sim 10^{-5}$), implying that capillarity dominates over inertia. It is also reasonable to neglect viscous effect (time scale of visco-capillarity, ~μs).[39] A dominance of capillarity means that the time scale for the stretching and contraction is limited by the kinetics of the potential-induced molecular reorganization of the films. As such, the time scale is independent of the tilt angle and the drop volume as long as the chosen conditions allow for the drop to be at rest after stretching and contraction. To confirm that molecular reorganization is the rate-limiting step, we performed electrochemical measurement (potential steps) on the LD-MHA film mounted inside an electrochemical cell and measured the decay in the charging current upon switching the applied bias between the two limiting values (Figure 5b). The time constants obtained from the exponential fits of the current decay ($I(t) = I_0 e^{-t/\tau}$) were found to be 1.68 ± 0.03 s upon switching from positive to negative applied potentials and 0.77 ± 0.02 s upon switching from negative to positive applied potentials, in reasonable agreement with the time constant for switching of the film inferred from the stretching and contraction of the drop on the inclined plane (Figure 5a). The larger time constant obtained from the analysis of drop motion (~3 s from Figure 5a) could be due to the intrinsic multi-step nature of the drop motion: time for molecular reorganization, drop deformation, and motion and the time necessary for the newly contacted SAM molecules to change the conformation as the drop spreads. On the other hand, the time constant from electrochemical potential-step measurement only accounts for a single step (molecular reorganization in the electrolyte solution). We have also performed a control experiment on an MHA crystalline monolayer in the same solution environment. The time constants were found to be 5.78 ± 0.01 ms upon switching the potential in both directions, which is 3 orders of magnitude smaller than we observed on low-density films in this work. As there is no molecular rearrangement within MHA crystalline monolayer, the diffusion-limited time scale is only associated with the rearrangement of the electrical double layer. In the cases of contraction followed by translational motion (finite acceleration at positive potential), we observed a decreased time constant; the drop in these cases is, however, still under the domination of surface tension force ($We \sim 10^{-2}$).

CONCLUSIONS

In conclusion, we have shown that low-density MHA films exhibit large change in contact angle hysteresis at different applied potentials. We have employed this external control over contact angle hysteresis as an "on-off" switch to realize drop motion on a homogenous surface. We have also shown that the stretching and contraction of the drop as it slides down the incline mimic the motion of an inchworm. Our results highlight an alternative and simple approach to control the dynamics of a liquid drop on a homogenous surface without patterning or fabrication. This work opens the door to controlling the motion of a drop by manipulating the pinning force versus other external driving forces, such as in pressure-driven flow.

ASSOCIATED CONTENT

Supporting Information

(1) Experimental setup for drop motion, (2) control of drop motion in a closed channel, (3) advancing and receding contact angle measurement, (4) current decay measurement of MHA crystalline film, and (5) movies of drop motion. This material is available free of charge via the Internet at http://pubs.acs.org.

AUTHOR INFORMATION

Corresponding Author

*E-mail: jfrechette@jhu.edu.

ACKNOWLEDGMENTS

This work was supported by the National Science Foundation under Grant No. CMMI-0748094 and CMMI-0709187.

REFERENCES

(1) Daniel, S.; Chaudhury, M. K.; Chen, J. C. *Science* **2001**, *291*, 633−636.
(2) Malvadkar, N. A.; Hancock, M. J.; Sekeroglu, K.; Dressick, W. J.; Demirel, M. C. *Nat. Mater.* **2010**, *9*, 1023−1028.
(3) Chu, K. H.; Xiao, R.; Wang, E. N. *Nat. Mater.* **2010**, *9*, 413−417.
(4) Yamada, R.; Tada, H. *Langmuir* **2005**, *21*, 4254−4256.
(5) Liu, M. J.; Nie, F. Q.; Wei, Z. X.; Song, Y. L.; Jiang, L. *Langmuir* **2010**, *26*, 3993−3997.
(6) Cheng, Z. J.; Feng, L.; Jiang, L. *Adv. Funct. Mater.* **2008**, *18*, 3219−3225.
(7) Ichimura, K.; Oh, S. K.; Nakagawa, M. *Science* **2000**, *288*, 1624−1626.
(8) Chen, L.; Liu, M. J.; Bai, H.; Chen, P. P.; Xia, F.; Han, D.; Jiang, L. *J. Am. Chem. Soc.* **2009**, *131*, 10467−10472.
(9) Li, C.; Guo, R. W.; Jiang, X.; Hu, S. X.; Li, L.; Cao, X. Y.; Yang, H.; Song, Y. L.; Ma, Y. M.; Jiang, L. *Adv. Mater.* **2009**, *21*, 4254−4258.
(10) Chaudhury, M. K.; Whitesides, G. M. *Science* **1992**, *256*, 1539−1541.
(11) Mettu, S.; Chaudhury, M. K. *Langmuir* **2011**, *27*, 10327−10333.

(12) Lai, Y. H.; Yang, J. T.; Shieh, D. B. *Lab Chip* **2010**, *10*, 499−504.
(13) Daniel, S.; Chaudhury, M. K.; de Gennes, P. G. *Langmuir* **2005**, *21*, 4240−4248.
(14) Yang, J.; Zhang, Z. Z.; Men, X. H.; Xu, X. H.; Zhu, X. T. *J. Colloid Interface Sci.* **2010**, *346*, 241−247.
(15) Zheng, Y. M.; Bai, H.; Huang, Z. B.; Tian, X. L.; Nie, F. Q.; Zhao, Y.; Zhai, J.; Jiang, L. *Nature* **2010**, *463*, 640−643.
(16) Shastry, A.; Case, M. J.; Bohringer, K. F. *Langmuir* **2006**, *22*, 6161−6167.
(17) Fang, G. P.; Li, W.; Wang, X. F.; Qiao, G. J. *Langmuir* **2008**, *24*, 11651−11660.
(18) Kataoka, D. E.; Troian, S. M. *Nature* **1999**, *402*, 794−797.
(19) Mettu, S.; Chaudhury, M. K. *Langmuir* **2008**, *24*, 10833−10837.
(20) Mettu, S.; Chaudhury, M. K. *Langmuir* **2010**, *26*, 8131−8140.
(21) Marinescu, M.; Urbakh, M.; Barnea, T.; Kucernak, A. R.; Kornyshev, A. A. *J. Phys. Chem. C* **2010**, *114*, 22558−22565.
(22) 't Mannetje, D. J. C. M.; Murade, C. U.; van den Ende, D.; Mugele, F. *Appl. Phys. Lett.* **2011**, *98*, 014102.
(23) Daniel, S.; Sircar, S.; Gliem, J.; Chaudhury, M. K. *Langmuir* **2004**, *20*, 4085−4092.
(24) Brunet, P.; Eggers, J.; Deegan, R. D. *Phys. Rev. Lett.* **2007**, *99*, 144501.
(25) Chen, Y. L.; Helm, C. A.; Israelachvili, J. N. *J. Phys. Chem.* **1991**, *95*, 10736−10747.
(26) Delmas, M.; Monthioux, M.; Ondarcuhu, T. *Phys. Rev. Lett.* **2011**, *106*, 136102.
(27) Macdougall, G.; Ockrent, C. *Proc. Royal Soc. London, Ser. A* **1942**, *180*, 0151−0173.
(28) Berejnov, V.; Thorne, R. E. *Phys. Rev. E* **2007**, *75*, 066308−1-6.
(29) ElSherbini, A. I.; Jacobi, A. M. *Prog. Colloid Polym. Sci.* **2004**, *128*, 57−62.
(30) Olivier, G. K.; Shin, D.; Gilbert, J. B.; Monzon, L. A. A.; Frechette, J. *Langmuir* **2009**, *25*, 2159−2165.
(31) Olivier, G. K.; Shin, D.; Frechette, J. *J. Electroanal. Chem.* **2010**, *639*, 50−58.
(32) Luo, M. X.; Frechette, J. *J. Phys. Chem. C* **2010**, *114*, 20167−20172.
(33) Berg, J. C. *Wettability*; CRC Press: New York, 1993.
(34) Lahann, J.; Mitragotri, S.; Tran, T. N.; Kaido, H.; Sundaram, J.; Choi, I. S.; Hoffer, S.; Somorjai, G. A.; Langer, R. *Science* **2003**, *299*, 371−374.
(35) Neumann, A. W.; Good, R. J. *J. Colloid. Interface Sci.* **1972**, *38*, 341−358.
(36) Priest, C.; Sedev, R.; Ralston, J. *Phys. Rev. Lett.* **2007**, *99*, 026103.
(37) Mugele, F.; Baret, J. C. *J. Phys.: Condens. Matter* **2005**, *17*, R705−R774.
(38) Gupta, R.; Sheth, D. M.; Boone, T. K.; Sevilla, A. B.; Frechette, J. *Langmuir* **2011**, *27*, 14923−14929.
(39) Nelson, W. C.; Sen, P.; Kim, C. J. *Langmuir* **2011**, *27*, 10319−10326.
(40) Li, F.; Mugele, F. *Appl. Phys. Lett.* **2008**, *92*, 244108.
(41) Gupta, R.; Olivier, G. K.; Frechette, J. *Langmuir* **2010**, *26*, 11946−11950.
(42) Mugele, F. *Soft Matter* **2009**, *5*, 3377−3384.
(43) Mugele, F.; Buehrle, J. *J. Phys.: Condens. Matter* **2007**, *19*, 375112.
(44) Bikerman, J. J. *J. Colloid Sci.* **1950**, *5*, 349−359.
(45) Furmidge, C. G. *J. Colloid Sci.* **1962**, *17*, 309−324.